Environmentally Friendly Mesoporous Material Derived From Thin-Film Transistor Liquid Crystal Display and Sandblasting and Its Application of Environmental Humidity Control

Ya-Wen Lin
National Taipei University of Technology
Wei-Hao Lee
National Taipei University of Technology
Hsiou-Hsuan Wang
National I-Lan University
Ta-Wui Cheng
National Taipei University of Technology
Chiao-Ying Chen
National I-Lan University
Lin Kae-Long (kllin@niu.edu.tw)
National I-Lan University https://orcid.org/0000-0002-8549-5721
Huang-Mu Lo
Chaoyang University of Technology

Research

Keywords: Mesoporous humidity control material, hydrothermal synthesis method, alkali fusion process, MCM-41, waste recycling

Posted Date: June 7th, 2021

DOI: https://doi.org/10.21203/rs.3.rs-509521/v1

Abstract

The preparation of an aluminum-mesoporous humidity controlling material (Al-MHCM) by hydrothermally synthesizing a mixture of thin-film transistor liquid crystal display (TFT-LCD) waste glass and sandblasting (SB) waste was studied; additionally, the remaining residue was completely reused. The synthesized Al-MHCM was analyzed, and its moisture controlling performance along with its pore and surface structure characteristics were determined. In addition, the influence of the hydrothermal synthesis temperature and silicon-to-aluminum molar ratio on the product was also studied. The characteristic analysis results of the product confirm that the product has a typical mesoporous structure, with a specific surface area of up to 1013 m^2/g, and the pore size distribution calculated by the BJH method is 3-4 nm with a pore volume of 0.97 cm^3/g. The ^{27}Al NMR analysis verifies that all the aluminum atoms of the product are in the form of tetrahedral aluminum (Td-Al) in the mesoporous Al-MHCM framework, which confirms the successful synthesis of Al-containing mesoporous MCM-41 materials. In addition, as the aluminum content increased, the water adsorption/desorption capacity of Al-MHCM also increased. Results show that when the hydrothermal synthesis temperature is 105°C, the product synthesized from a mixture with a silicon-to-aluminum molar ratio of 41.8 exhibits excellent performance (91.45 m^3/ m^3) in terms of the equilibrium moisture content and moisture adsorption capacity. Al-MHCM, which can be synthesized at a low cost, can be used as a humidity controlling material for adjusting the relative humidity of indoor environmental spaces. Thus, this study provides a novel method for producing Al-MHCM to use as a future humidity-controlling building material.

1 Introduction

In the early 1990s, scientists at Mobil Petroleum Corporation discovered an ordered mesoporous silicate/aluminosilicate material, which they called the M41S series [1–3]. Since then, a series of studies have been conducted, in which the influence of the concentration of the surface active agent on the prepared mesoscopic particles was studied, and three structural arrangements were determined: a hexagonal structure - Mobil Composition of Matter No. 41 (MCM-41), a cubic structure - Mobil Composition of Matter No. 48 (MCM- 48) and a layered structure - Mobil Composition of Matter No. 50 (MCM-50). Among them, MCM-41 is the most studied mesoporous material because of its good thermal, hydrothermal and hydrolytic stability along with its high surface area and pore volume [4–6]. In addition, MCM-41 can prevent the agglomeration of a supported metal oxide by forming a bond between the surface silicon hydroxyl bridge and the deposited oxide [7]. It has been reported that the incorporation of Al into the MCM-41 framework can provide the resulting Al-MCM-41 material with Bronsted acid sites while exhibiting good adsorption affinity, thereby broadening its potential application [8–9]. However, the cost of silicon dioxide precursors commonly used in the synthesis process (such as sodium silicate or silicon alkoxide) represents a major problem in the use of such materials in regard to economic and environmental considerations [10]. Therefore, some research has been conducted to develop mesoporous silica using low-cost silica resources, including fly ash [11], wheat stem ash [12] and packaging resin waste [13]. Despite this plethora, reports on MCM-41mesoporous material synthesis from thin-film

transistor liquid crystal display waste glass and sandblasting waste are still scarce in literature. In the optoelectronic industry, a large amount of thin film transistor liquid crystal display waste glass (TFT-LCD waste glass) is generated during panel manufacturing, assembly and cutting. In addition, sandblasting waste (SB waste) is the surface etching process after the silicon wafer is cut, and the surface of the silicon material is optimized through the use of abrasive sand, thereby mass production of SB waste in the upstream factory of the solar cell module. In the past, most of these wastes were treated by incineration or landfill, thus wasting valuable materials. Therefore, from an environmental and economic point of view, a cleaner process to add value and provide resource reuse and safe disposal research for solid waste is of great significance. In addition, a mesoporous material of MCM-41 can be prepared by a variety of synthetic methods, such as a hydrothermal treatment [14], a sol-gel method [15], co-condensation method [16], and an impregnation method [17].The hydrothermal treatment method is the preferred method because it is simple and the operational complexity is low; furthermore, it has been reported that the hydrothermal treatment can increase the structural stability, acidity, activity and surface area of the mesoporous material [18].

Taiwan has a subtropical island climate, with warm and humid weather conditions year round; thus, the hot climate and high humidity of Taiwan provide ideal conditions for mold. According to the literature, the most comfortable range of relative humidity for the human body is 40–70% [19]; additionally, excessively dry or humid environments are not conducive to human health and life [20]. Therefore, to achieve effective humidity control while also avoiding the use of energy-consuming methods, such as mechanical air conditioning, the development of new and energy-free indoor humidity control technologies has been explored to save energy and provide healthy living environments [21–22]. If low-cost silicon dioxide resources (thin-film transistor liquid crystal display waste glass and sandblasting waste) can be used to produce mesoporous MCM-41 materials for the preparation of Al-MHCM with humidity controlling performance, then the humidity of the environment can be adjusted while decreasing the amount of pollution in the environment. With no need to consume energy or use other equipment, as long as the original capillary phenomenon of the mesoporous material is used, the designed Al-MHCM exhibits moisture absorption and desorption characteristics, thereby achieving moisture control. Therefore, the purpose of this research is to confirm the application of MCM-41 as a humidity controlling material. This study is the first attempt to measure the influence of various temperatures and Si/Al molar ratios on the pore structure and surface characteristics of Al-MHCM produced from waste materials and its performance toward environmental humidity control. In addition, the feasibility of producing zeolite, from the remaining residue of the primary synthesis, was studied to achieve the goal of zero environmental resource waste.

2 Materials And Methods

2.1. Materials (TFT-LCD waste glass and SB waste)

The TFT-LCD waste glass and SB waste were provided by the Central Taiwan Resource Recycling Plant

pectively. These wastes were dried, ground and sieved to

achieve a particle size ≤ 74 μm. As shown in Table 1, its chemical composition was measured and analyzed by X-ray fluorescence (XRF) spectroscopy. The main components of the TFT-LCD waste glass were SiO_2, Al_2O_3 and CaO, which accounted for 69.70, 15.30 and 8.45%, respectively, and the molar ratio of SiO_2 to Al_2O_3 was approximately 4.5. The main components of the SB waste were SiO_2 and Al_2O_3, which accounted for 70.10 and 13.90%, respectively. The molar ratio of SiO_2 to Al_2O_3 was calculated to be approximately 5.0. Among them, TFT-LCD waste glass mainly came from material cut from glass substrates, and SiO_2 and Al_2O_3 were the main bodies of the glass network structure, thereby providing an abundance of SiO_2 and Al_2O_3. The mineralogical phase analysis of TFT-LCD waste glass and SB waste using XRD is shown in Fig. 1. TFT-LCD waste glass had an amorphous structure inside, so there was no obvious diffraction peak. SB waste produced diffraction peaks of silicon oxide, aluminum oxide and Cu3Ge.

Table 1
Chemical composition of materials.

Composition (%)	SiO_2	Al_2O_3	Fe_2O_3	CaO	MgO	TiO_2	SiO_2/ Al_2O_3
TFT-LCD Waste Glass	69.70	15.30	0.18	8.45	0.77	0.22	4.5
SB Waste	70.10	13.90	7.72	1.31	-	5.82	5.0

2.2. Extraction of SiO_2 and Al_2O_3 in an alkaline melting process

TFT-LCD waste glass and SB waste were mixed together, and silicate and aluminosilicate were extracted through an alkali melting temperature of 450°C with the addition of a 1.5 proportion of NaOH. The molten material was crushed to obtain powder. The powder was mixed with distilled water at different ratios to dissolve the aqueous solution containing SiO_2 and Al_2O_3 and then filtered to obtain sodium aluminosilicate solutions with SiO_2/Al_2O_3 molar ratios of 26, 41.8 and 56.3.

2.3. Synthesis of Al-mesoporous humidity controlling material (Al-MHCM)

Al-MHCM was synthesized by using the hydrothermal method. First, the required amount of CTAB was dissolved in 30 mL of deionized water and ammonia to form a template solution. Sodium aluminosilicate solutions with the different SiO_2/Al_2O_3 molar ratios stated above were slowly added to the CTAB template solution while stirring. Sulfuric acid (1 M) was used to adjust the pH of the dispersion, and then the dispersion was stirred continuously for 2 h. The mixed solution was then transferred to a stainless steel autoclave (200 mL) lined with Teflon. The mixed solution was heated at different hydrothermal temperatures (90, 105, 120°C) for 48 h. Next, the obtained product was washed with distilled water, filtered, and then dried in an oven at 105°C overnight. Finally, the obtained product was calcined up to 550°C at a heating rate of 5°C/min in air to burn off the surfactant from the matrix. The obtained

2.4. Test and methods

The used TFT-LCD waste glass and SB waste were analyzed by an XRF fluorescence analyzer (RIX 2000) to obtain the chemical element composition of the raw materials. The pore structure of Al-MHCM was determined by X-ray powder diffraction (D8AXRD) to identify the crystalline phases in the material. Diffraction data were collected between 2θ = 1–8°. Scanning electron microscopy (SEM; American FEI company (Nova Nanosem 230)) was used to characterize the surface morphology and structural changes of the sample. A solid-state ^{27}Al NMR spectrum of Al-MHCM was obtained. A nitrogen adsorption and desorption instrument (Tristar 3000) was used to obtain isotherms, and the surface area was measured by the Brunauer-Emmett-Teller (BET) method; finally, the total pore volume and pore diameter were calculated by the BJH method.

2.5. Moisture adsorption/desorption test

The moisture adsorption/desorption test was performed in accordance with the method for measuring the equilibrium moisture content in Japanese Industrial Standards JIS A 1475. First, the test body was dried in an oven at 105°C for 24 h, and its constant weight was recorded. Next, the sample was placed in a constant temperature and humidity controller, and the relative humidity was changed to 10, 33, 55, 75, 85, and 95% at a fixed temperature of 23°C. The constant weight of adsorption (from low to high) and desorption (from high to low) of the sample was recorded at this relative humidity. Finally, the moisture absorption per unit area of mesoporous Al-MHCM was obtained at different times. The standard of the Japanese Industrial Regulations JIS A 1470 humidity controlling building materials regulations was verified, and the standard value, based on the average equilibrium moisture content (> 5 kg/m^3), was evaluated.

3 Results And Discussion

3.1. Heavy metal leaching concentration of the raw materials

The leaching concentration of heavy metals that passed the toxicity characteristic leaching procedure (TCLP) test is shown in Table 2. In addition, the total leaching concentration of heavy metals was also analyzed, and each material was subjected to a heavy metal leaching test. The concentrations of the leached heavy metals from each material was measured by flame atomic absorption spectrometer (FL-AAS). The analysis results of the total amount of heavy metals show that the TFT-LCD waste glass is dominated by Zn, with a content of 160 mg/kg, and the main source are the wires in the panel etching tank. The predominant heavy metal in the SB waste is mainly Cr, which is caused by the SB waste from the coating treatment of a solar panel, and its content is 90 mg/kg, followed by the contents of Zn and Cu, which are 65 and 25 mg/kg, respectively. The experimental results show that the leaching concentrations of TFT-LCD waste glass and SB waste all met Taiwan's EPA regulatory limits.

Table 2
Heavy metal leaching concentration tested by TCLP.

Total Metal (mg/kg)	Pb	Cr	Cu	Zn	Cd	Ni
TFT-LCD Waste Glass	N.D.	N.D.	N.D.	160	N.D.	N.D.
SB waste	N.D.	90	25	65	N.D.	10
TCLP (mg/L)	Pb	Cr	Cu	Zn	Cd	Ni
TFT-LCD Waste Glass	N.D.	N.D.	N.D.	0.1	N.D.	N.D.
SB waste	N.D.	N.D.	N.D.	0.8	N.D.	N.D.
Regulatory Limits	5.00	5.00	15.00	-	1.00	-
N.D.:Pb□0.015 mg/L;□Cd□0.021 mg/L□Ni□0.112 mg/L						

3.2. Crystal phase analysis of Al-MHCM

Figure 2 shows the XRD diffraction patterns of Al-MHCM synthesized at different temperatures and different Si/Al molar ratios. The XRD pattern of Al-MHCM shows that the main diffraction peaks are at 2.34 and 2.42° along with 3.90 and 4.50°, which correspond to the characteristic $d_{(100)}$, $d_{(110)}$ and $d_{(200)}$ peaks of MCM-41, respectively [23]. With the increase in the Si/Al molar ratio, the two higher-order hexagonal structure peaks ($d_{(110)}$ and $d_{(200)}$) tend to increase. At lower Si/Al ratios, the main characteristic peaks are slightly shifted, which is mainly due to the 2θ angle shift caused by the high aluminum content in the source material; this result means that Al atom doping in the crystal lattice changes the crystallinity of the product and causes poor sorting. Therefore, with increasing aluminum content, the intensity of the diffraction peak gradually decreases, indicating that the order of the structure decreases [24–25]. In addition, it can be found from the change in the hydrothermal temperature that when the temperature increased from 90 to 120°C, the main characteristic peak $d_{(100)}$ has relatively stable crystallinity. The characteristic peaks (d_{110} and d_{200}) representing the hexagonal structure also have a tendency to gradually form as the hydrothermal temperature increased because when the hydrothermal temperature increased, the balance between the solid and liquid phases of the initial gel is destroyed; this imbalance accelerates the aggregation of silicate species on the micelle surfaces. Therefore, a high hydrothermal temperature is conducive to the formation of a well-ordered MCM-41 structure because the high temperature will accelerate the condensation rate of silicate on the silicon dioxide wall [26].

3.3. Solid-state ^{27}NMR analysis of Al-MHCM

The ^{27}Al NMR spectrum was used to track the change in the position of Al added to Al-MHCM. All the spectra of the current Al-MHCM material are dominated by the signal of the tetrahedral-coordinated aluminum (Al^{IV}) species with ^{27}Al = 53 ppm (Fig. 3), and the weak signal at ^{27}Al = 0 ppm is due to the octahedral-coordinated aluminum (Al^{VI}) species (Fig. 3(c)) [27]. The appearance of Al^{VI} species is usually related to the Lewis acid on the surface, and the strength will increase with an increasing content of Al^{IV}

species [28]. However, when the Si/Al molar ratio is lower (Fig. 3 (a)-(b)), more Al atoms (Al^{VI}) are introduced into the silicon dioxide framework, thereby generating and enhancing the Al^{IV} signal. It is well known that Al^{IV} can enhance the acid strength of adjacent SiOH groups, thereby forming Brønsted acid sites (BAS) with high catalytic activity [29]. In addition, from the area content of the tetrahedral-coordinated aluminum (Al^{IV}) species, it can be seen that when the hydrothermal temperature is low (90°C), the occupied area is between 38.50-52.02%, and when the hydrothermal temperature is increased to 105°C, the area occupied by Al^{IV} species is between 52.67–59.61%. In addition, when the hydrothermal temperature is 120°C, the area occupied by species at 53 ppm increased to 54.98–67.17%. These results show that as the hydrothermal temperature increased, Al^{VI} can be more effectively converted to a tetrahedron (Td-Al), which is the form that enters the skeleton.

3.4. SEM analysis of Al-MHCM

In this study, the microstructure changes of Al-MHCM were observed through FE-SEM. The morphology of the Al-MHCM material at a 50,000x magnification is shown in Fig. 4. During the hydrothermal treatment under alkaline conditions (pH = 10), silicate and aluminosilicate are extracted from the TFT-LCD waste glass and SB waste. Then, the extracted silicate and aluminosilicate are mixed with the CTAB surfactant to form a mesoporous silica material similar to MCM-41 [30]. In addition, it can be seen that even after the calcination process (550°C), the macrostructure of Al-MHCM remains intact, thus confirming the high thermal stability of Al-MHCM [31]. The morphology of Al-MHCM is clearly observed as round nanoparticles, and the appearance of the particles is mainly spherical. From the observations in Fig. 4(a)-(c), when the Si/Al ratio is 26 and the hydrothermal temperature is 90–120°C, the size distribution of Al-MHCM crystals is approximately 0.13–0.22 μm. When the Si/Al ratio is increased to 41.8, the crystal size is approximately 0.11–0.40 μm. At the highest Si/Al ratio (56.3), the Al-MHCM crystal size distribution is approximately 0.22–0.60 μm. This phenomenon shows that the increase in hydrothermal temperature causes the crystal size to decrease significantly. According to the study by Grisdanurak et al., this increase in crystal size was mainly due to the increased synthesis temperature and rapid hydrolysis reaction that affected the uniformity of the generated particles [32]. In addition, Ekloff et al. stated that the difference between products obtained by the same synthesis method was due to the formation of delayed structures due to changes in the reaction medium pH or the occurrence of uneven precipitation [33].

3.5. N_2 isothermal adsorption-desorption of Al-MHCM

The N_2 adsorption-desorption phenomenon provides a technique for determining the surface area, pore volume and pore size distribution. The N_2 isotherm adsorption-desorption curve is shown in Fig. 5. All the synthesized Al-MHCM junctions exhibit a type-IV nitrogen adsorption-desorption isotherm. According to the IUPAC nomenclature, this is a typical feature of homogeneous mesoporous materials [34]. The isotherm shows the following three stages: when the low relative pressure is 0.2–0.3, the monolayer adsorption of nitrogen on the mesoporous wall is observed; and when the relative pressure is 0.3–0.4, a sharp increase occurs under the same parameter conditions with different Si/Al ratios. This is

characteristic of capillary condensation in mesopores, which shows a narrow hysteresis loop. Finally, when the relative pressure is 0.5–0.9, the synthesized Al-MHCM shows slightly tilted plateau, which is caused by multilayer adsorption on the outer surface of particles [35]. In addition, when the Si/Al ratio is 26, 41.8 and 56.3, the specific surface area ranges from 506–587, 733–795 and 781–1013 m^2/g, respectively. The adsorption-desorption characteristics for all samples are typical of mesoporous materials, indicating that mesoporous materials have better adsorption performance.

Figure 6 shows the total pore volume and pore diameter calculated by the N_2 adsorption-desorption measurements and the BJH method and are listed in Table 3. The pore size distribution curves of all Al-MHCM shown in Fig. 6 are unimodal and belong to a narrow range of mesopores that are approximately 3–4 nm, indicating the existence of mesopores in the particles. Thus, this result confirms the successful synthesis of a uniform mesoporous material, and is consistent with the BJH method for calculating the pore size (Table 3). In addition, Fig. 6 (a) shows that when the Si/Al ratio is 26, the pore volume of the synthesized Al-MHCM is 0.4–0.5 cm^3/g. When the Si/Al ratio is increased to 56.3, the pore volume is increased to 0.9–1.4 cm^3/g. Based on the above knowledge, the increase in the Si/Al ratio and hydrothermal temperature can form an ordered mesoporous structure. The pore volume and specific surface area of the synthesized Al-MHCM increase accordingly, with the highest pore volume being 0.97 cm^3/g, and the highest specific surface area being 1013 m^2/g (Al-$MHCM_9$). The results of Sohrabnezhad and Mooshangaie show that adding metal (such as Ag/AgBr) to an MCM-41 material will increase the pore size and pore volume, which indicated that some of the metal was dispersed on the inner pore surfaces of the MCM-41 material [36].

Table 3
The pore structure characteristics of Al-MHCM with 26, 41.8, and 56.3 Si/Al molar ratio.

Sample	Si/Al[a] Molar Ratio	Hydrothermal Temperature (°C)	Surface Area (m^2/g)	Pore Volume (cm^3/g)	Pore Diameter (nm)	d_{100}[a] (nm)	a0[b] (nm)	W.t[c] (nm)
Al-MHCM$_1$	26	90	511	0.51	3.52	3.67	4.24	0.72
Al-MHCM$_2$		105	506	0.53	3.63	3.85	4.45	0.82
Al-MHCM$_3$		120	587	0.65	3.87	4.06	4.69	0.82
Al-MHCM$_4$	41.8	90	795	0.73	3.40	3.67	4.24	0.84
Al-MHCM$_5$		105	733	0.62	3.04	3.67	4.24	1.20
Al-MHCM$_6$		120	780	0.71	3.28	4.06	4.69	1.41
Al-MHCM$_7$	56.3	90	781	0.74	3.26	4.06	4.69	1.43
Al-MHCM$_8$		105	870	0.78	3.18	4.06	4.69	1.51
Al-MHCM$_9$		120	1013	0.97	3.05	3.85	4.45	1.40

[a] Unit Cell Distance ; [b] Unit Cell Constant = $2d_{100}/\sqrt{3}$; [c] Wall Thickness (W.t.)= (a_0) - (Pore Diamrter)

3.6. The 24 h equilibrium moisture content curve of Al-MHCM

Figure 7 shows the equilibrium moisture content of Al-MHCM at different relative humidities (RHs). The solid line in Fig. 7 shows the process of water vapor adsorption, and the dotted line is the process of water vapor desorption. The results show that the equilibrium water contents of all samples increase with increasing RH. However, there is a significant difference in the equilibrium moisture content in the material, especially when the relative humidity is high (75 to 95%). Figure 7 shows that when the Si/Al ratio is 26, the RH of the synthesized Al-MHCM is 95%, the equilibrium moisture content is in the range of 65.20–76.60 m^3/m^3 (Fig. 7 (a)). When the Si/Al ratio is 41.8, the highest equilibrium moisture content is shown to be in the range of 81.34–91.45 m^3/m^3 (Fig. 7(b)). In addition, when the Si/Al ratio is 56.3 and the RH of the synthesized Al-MHCM is 95%, the equilibrium moisture content is 69.63–75.15 m^3/m^3 (Fig. 7 (c)). These results show that the adsorption characteristics are closely related to the specific surface area and pore size. In the process of water vapor absorption and desorption, the pore size of Al-MHCM is significantly related to capillary condensation [37]. In addition, Jansen et al. observed that water saturation increased with relative humidity in a relatively nonlinear manner; furthermore, they found that the diffusion coefficient did not depend on the water concentration itself because there was no difference

in the diffusion rate between absorption and desorption [38]. In addition, when the low hydrothermal synthesis temperature is 90°C, the equilibrium moisture content of Al-MHCM at 95% RH is 73.19 m^3/m^3, and when the hydrothermal temperature is increased to 120°C, the equilibrium moisture content increased significantly to 76.60 m^3/m^3 (Fig. 7(a)). Moreover, the adsorption-desorption curve shows a hysteresis loop. Since the inner wall of the pore is in a wet state after the loss of water during the dehumidification process, the contact angle of the water molecules on the inner wall of the pore is small, thereby delaying the desorption effect. In contrast, in the process of moisture absorption, the inner wall of the dry pore has a better moisture absorption effect with its large water contact angle. The above results show that the change in the Si/Al ratio exhibits no obvious difference in regard to the change in equilibrium moisture content, while an increase in the hydrothermal temperature can destroy the balance between the solid and liquid phases of the initial gel; thus, the concentration of silicate and aluminosilicate in the liquid phase results in the aggregation of silicate species on the microcell surface. Aggregation promotes the crystallization process and increased the pore structure and specific surface area of Al-MHCM; therefore, the equilibrium moisture content gradually increased.

3.7. Feasibility of synthesizing microporous zeolite

In this study, after the alkaline fusion process and extraction of SiO_2 and Al_2O_3, we tried to use the remaining residue as a starting material for a direct hydrothermal synthesis of zeolite with a one-pot hydrothermal method. Through the use of a 3 M NaOH solution as the alkali treatment, the formation and crystal phase influence of the synthesized microporous zeolite at different hydrothermal temperatures (100, 150, 200°C) were discussed; furthermore, this process is expected to achieve the purpose of completely reusing the remaining residue. Figure 8 shows the XRD pattern. It can be seen from Fig. 8 that when the silicon-to-aluminum ratio is fixed, comparing different temperatures will produce different types and crystal phases of zeolite. The results show that it is mainly zeolites such as analcime, sodalite, and cancrinite [39]. When the hydrothermal temperature is 200°C, cancrinite clearly appears at $2\theta = 14.22$ and 27.18°. Additionally, the alkaline melting process can effectively separate the SiO_2 and Al_2O_3 supernatant liquid and the remaining residue. Thus, the obtained supernatant liquid is mainly silicate and aluminosilicate, which can synthesize valuable Al-MHCM molecular sieves, while the remaining residue can be recycled and activated into microporous zeolite, showing potential for secondary recycling.

4. Conclusions

….. This study uses TFT-LCD waste glass and SB waste to produce Al-MHCM. The microscopic characteristics of the synthesized mesoporous Al-MHCM are established by changing the Si/Al ratio and hydrothermal temperature and analyzing the moisture absorption performance of each sample. The TCLP dissolution test results show that the heavy metal leaching amount of each material meets the legal standards, so TFT-LCD waste glass and SB waste have the potential to be recycled. The XRD analysis shows that a high hydrothermal temperature is conducive to the formation of a well-ordered structure. The ^{27}Al-NMR analysis shows that Al^{VI} can be converted more effectively to a tetrahedron (Td-

n. These results also show that the increase in hydrothermal

temperature makes the crystal size significantly smaller. However, the crystal size increased as the Si/Al ratio increased, and the pore volume and specific surface area of the synthesized Al-MHCM increase accordingly; the highest pore volume is 0.97 cm^3/g, and the highest specific surface area is 1013 m^2/g (Al-$MHCM_9$). These results show that the addition of Al metal to Al-MHCM will increase the pore size and pore volume; therefore, some of the metal is dispersed on the inner pore surface of the material. From the equilibrium moisture content test, it is found that during the absorption and desorption of water vapor, the pore size of Al-MHCM is significantly related to the capillary condensation, and it is expected that the adsorption characteristics are closely related to the specific surface area and pore size. Finally, when the Si/Al ratio is 41.8, the highest equilibrium moisture content is shown to be 91.45 m^3/m^3.

Declarations

Availability of data and materials

All data generated or analyzed during this study are available from the corresponding author upon request.

Competing interests

The authors declare they have no competing interests.

Funding

This work was supported by Ministry of Science and Technology of the Republic of China, Taiwan, for supporting this research financially (Contract No. MOST-107-2221-E-197-002-MY3).

Authors' contributions

Ya-Wen Lin: Writing - original draft. Methodology. onceptualization. Wei-Hao Lee: Supervision. Hsiou-Hsuan Wang: Supervision. Ta-Wui Cheng: Supervision. Chiao-Ying Chen: Validation, Investigation, Methodology. Kae-Long Lin: Resources, writing-commenting and editing. All authors reviewed and approved the final manuscript.

Acknowledgements

This work was supported by Ministry of Science and Technology of the Republic of China, Taiwan, for supporting this research financially (Contract No. MOST-107-2221-E-197-002-MY3).

Authors' information (optional)

References

1. Beck JS, Vartuli JC, Roth WJ, Leonowicz ME, Kresge CT, Schmitt KD, et al. A new family of mesoporous molecular sieves prepared with liquid crystal templates. J. Am. Chem. Soc. 1992;114:10834-10843.
2. Kresge CT, Leonowicz ME, Roth WJ, Vartuli JC, Beck JS. Ordered mesoporous molecular sieves synthesized by a liquid-crystal template mechanism. Nature. 1992;359:710-712.
3. Kresge CT, Vartuli JC, Roth WJ, Leonowicz ME. The discovery of ExxonMobil's M41S family of mesoporous molecular sieves. Stud Surf Sci Catal. 2004;148:53-72.
4. Woszuk A, Panek R, Madej J, Zofka A, Franus W. Mesoporous silica material MCM-41: Novel additive for warm mix asphalts. J. Mater. Civ. Eng. 2018;183:270-274.
5. Arica TA, Ayas E, Arica MY. Magnetic MCM-41 silica particles grafted with poly(glycidylmethacrylate) brush: Modification and application for removal of direct dyes. Microporous Mesoporous Mater. 2017;243:164-175.
6. Rabie AM, Shaban M, Abukhadra MR, Hosny R, Ahmed SA, Negm NA. Diatomite supported by CaO/MgO nanocomposite as heterogeneous catalyst for biodiesel production from waste cooking oil. J. Mol. Liq. 2019;279:224-231.
7. Ghorbani F, Younesi H, Mehraban Z, Celik MS, Ghoreyshi AA, Anbia M. Preparation and Characterization of Highly Pure Silica from Sedge as Agricultural Waste and its Utilization in the Synthesis of Mesoporous Silica MCM-41. J Taiwan Inst Chem Eng. 2013;44:821-828.
8. Salam MA, AbuKhadra MR, Mohamed AS, Effective oxidation of methyl parathion pesticide in water over recycled glass based-MCM-41 decorated by green Co_3O_4 Environ. Pollut. 2020;259:113874.
9. Ściubidło A, Majchrzak-Kucęba I. Exhaust gas purification process using fly ash-based sorbents. Fuel. 2019;258:116126.
10. Sohrabnezhad S, Jafarzadeh A, Pourahmad A. Synthesis and characterization of MCM-41 ropes.Mater. Lett. 2018;212:16-19.
11. Liou TH. A green route to preparation of MCM-41 silicas with well-ordered mesostructure controlled in acidic and alkaline environments. Chem. Eng. J. 2011;171:1458-1468.
12. Hussain M, Song SK, Ihm SK. Synthesis of hydrothermally stable MCM-41 by the seed crystallization and its application as a catalyst support for hydrodesulfurization. Fuel. 2013;106:787-792.
13. Roik NV, Belyakova LA. Sol–gel synthesis of MCM-41 silicas and selective vapor-phase modification of their surface. J Solid State Chem. 2013;207:194-202.
14. Mamontov GV, Gorbunova AS, Vyshegorodtseva EV, Zaikovskii VI, Vodyankina OV. Selective oxidation of CO in the presence of propylene over Ag/MCM-41 catalyst. Catal. Today. 2019;333:245-250.
15. Lourenço JP, Fernandes A, Henriques C, Ribeiro MF. Al-containing MCM-41 type materials prepared by different synthesis methods: Hydrothermal stability and catalytic properties. Microporous Mesoporous Mater. 2006;94:56-65.

16. Arundel AV, Sterling EM, Biggin JH, Sterling TD. Indirect health effects of relative humidity in indoor environments. Environ. Health Perspect. 1986;65:351-361.
17. Chen Z, Qin MH, Yang J. Synthesis and characteristics of hygroscopic phase change material: Composite microencapsulated phase change material (MPCM) and diatomite. Build. Res. Inf. 2015;106:175-182.
18. Hu ZB, Zheng SL, Jia MZ, Dong XB, Sun ZM. Preparation and characterization of novel diatomite/ground calcium carbonate composite humidity control material. Adv Powder Technol. 28 (2017) 1372-1381.
19. Liu YY, Jia HW, Zhang GX, Sun ZM, Pan YT, Zheng SL. Synthesis and humidity control performances of natural opoka based porous calcium silicate hydrate. Adv Powder Technol. 2019;30:2733-2741.
20. Deekamwong K, Kaiyasuan C, Jitcharoen J, Wittayakun J. Influence of gel composition and microwave-assisted hydrothermal time in MCM-41 synthesis. Mater. Chem. Phys. 2017;201:384-390.
21. Rosales Hernández MC, Mendieta Wejeb e JE, Vázquez Alcántara JI, Miranda Ruvalcaba R, García Serrano LA, Trujillo Ferrara J. Immobilization of cytochrome P-450 on MCM-41 with different silicon/aluminum ratios. Microporous Mesoporous Mater. 2005;80:25-31.
22. Hea D, Bai C, Jiang C, Zhou T. Synthesis of Titanium Containing MCM-41 and Its Application for Catalytic Hydrolysis of Cellulose. Powder Technol. 2013;249:151-156.
23. Wang ZC, Ling HJ, Shi J, Stampfl C, Yu AB, Hunger M, Huang J. Acidity enhanced [Al]MCM-41 via ultrasonic irradiation for the Beckmann rearrangement of cyclohexanone oxime to □-caprolactam. J Catal 2018;358:71-79.
24. Wang Z, Jiang Y, Rachwalik R, Liu Z, Shi J, Hunger M, Huang J. One-step room-temperature synthesis of [Al]-MCM-41 materials for the catalytic conversion of phenylglyoxal to ethylmandelate. ChemCatChem. 2013;5:3889-3896.
25. Jiang YJ, Huang J, Dai WL, Hunger M. olid-state nuclear magnetic resonance investigations of the nature, property, and activity of acid sites on solid catalysts. Solid State Nucl Magn Reson. 2011;39:116-141.
26. Sohrabnezhad S, Mooshangaie SD. In situ fabrication of n-type Ag/AgBr nanoparticles in MCM-41 with rice husk (RH/MCM-41) composite for the removal of Eriochrome Black-T. Mater. Sci. Eng. C. 2019;240:16-22.
27. Carmo Jr AC, de Souza LKC, da Costa CEF, Longo E, Zamian JR, da Rocha Filho GN. Production of biodiesel by esterification of palmitic acid over mesoporous aluminosilicate Al-MCM-41. Fuel 2009;88:461-468.
28. Grisdanurak N, Chiarakorn S, Wittayakun J. Utilization of mesoporous molecular sieves synthesized from natural source rice husk silica to Chlorinated Volatile Organic Compounds (CVOCs) adsorption. Korean J Chem Eng. 2003;20:950-955.
29. Ekloff GS, Rathouský J, Zukal A. Controlling of morphology and characterization of pore structure of ordered mesoporous silicas. Microporous Mesoporous Mater. 1999;27:273-285.

30. Sing KSW, Everett DH, Haul RAW, Moscow L, Apierotti R, Rouquerol T. Reporting Physisorption Data for Gas/Solid Systems with Special Reference to the Determination of Surface Area and Porosity. Pure Appl. Chem. 1985;57:603-619.
31. Souza MJB, Araujo AS, Pedrosa AMG. Textural features of highly ordered Al-MCM-41 molecular sieve studied by X-ray diffraction, nitrogen adsorption and transmission electron microscopy. Mater. Lett. 2006;60:2682-2685.
32. Tian W, Du B, Shui A, Ke SJ, Shan QL, He C, Ma J. Template-free preparation of humidity self-regulating silica-based mesoporous oxide from volcanic ash. J Solgel Sci Technol. 2002;94:416-424.
33. Xie HH, Gong GC, Wu Y. Investigations of equilibrium moisture content with Kelvin modification and dimensional analysis method for composite hygroscopic material. Constr Build Mater. 2017;139:101-113.
34. Jansen KMB, Zhang MF, Ernst LJ, Vu DK, Weiss L. Effect of temperature and humidity on moisture diffusion in an epoxy moulding compound material. Microelectronics J. 2020;107: 113596.
35. García-Villén F, Flores-Ruíz E, Verdugo-Escamilla C, Huertas FJ. Hydrothermal synthesis of zeolites using sanitary ware waste as a raw material. Clays Clay Miner. 2018;160:238-248.
36. Zeng W, Qian XF, Yin J, ZK Zhu. The drug delivery system of MCM-41 materials via co-condensation synthesis. Mater. Chem. Phys. 2006;97:37-441.
37. Zheng S, Li ZP, Gao L. Synthesis and characterization of TiOxNy assembled in oxynitrided mesoporous silica MCM-41. Mater. Chem. Phys. 2004;85:195-200.
38. Gomes Jr WA, Cardoso LAM, Gonzaga ARE, Aguiar LG, Andrade HMC. Influence of the extraction methods to remove organic templates from Al-MCM-41 molecular sieves. Mater. Chem. Phys. 2005;93:133-137.
39. Yuan ZY, Ma HT, Luo Q, Zhou WZ. Synthesis and characterization of manganese-modified MCM-41. Mater. Chem. Phys. 2003;77:299-303.

Figures

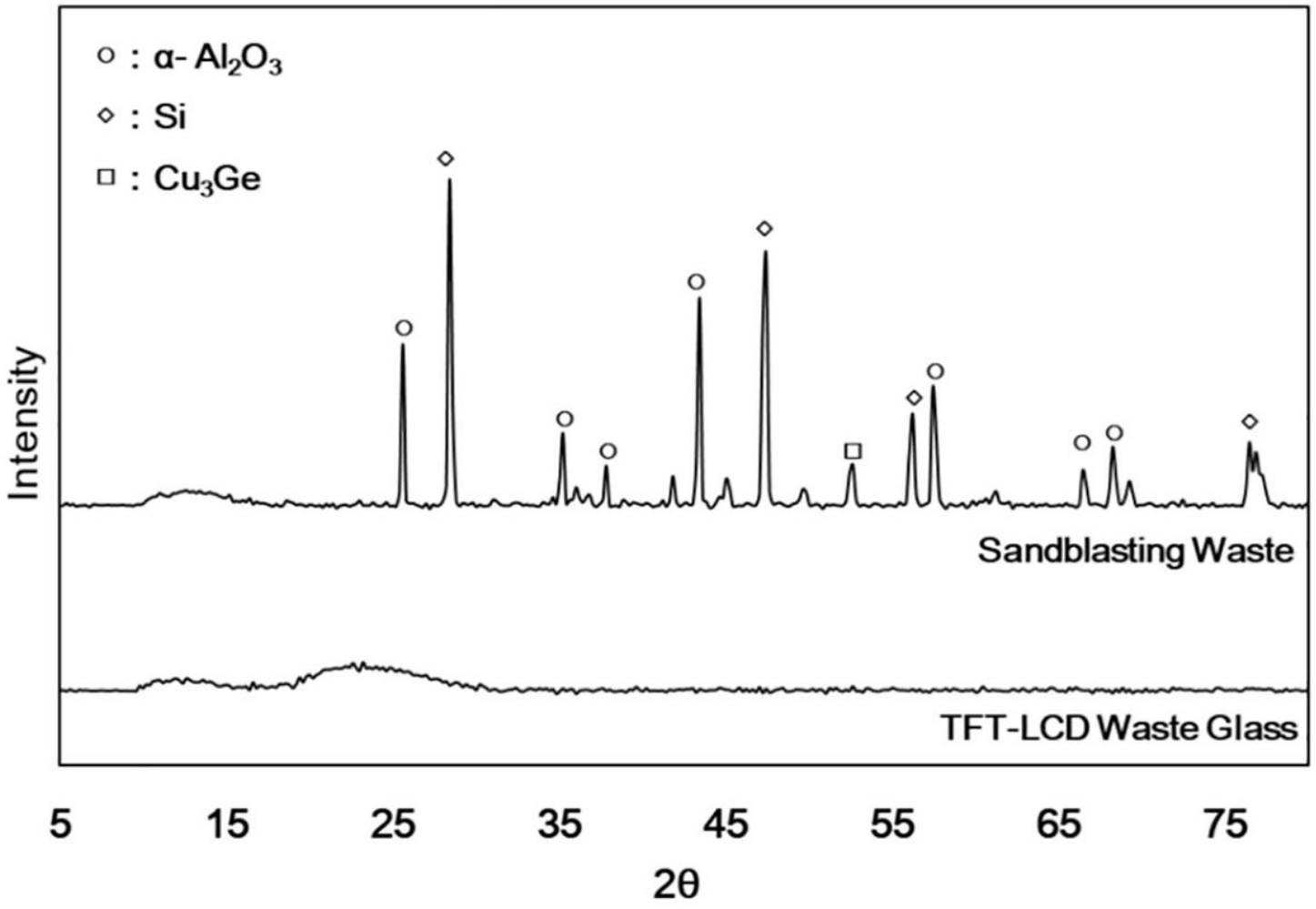

Figure 1

XRD patterns of materials.

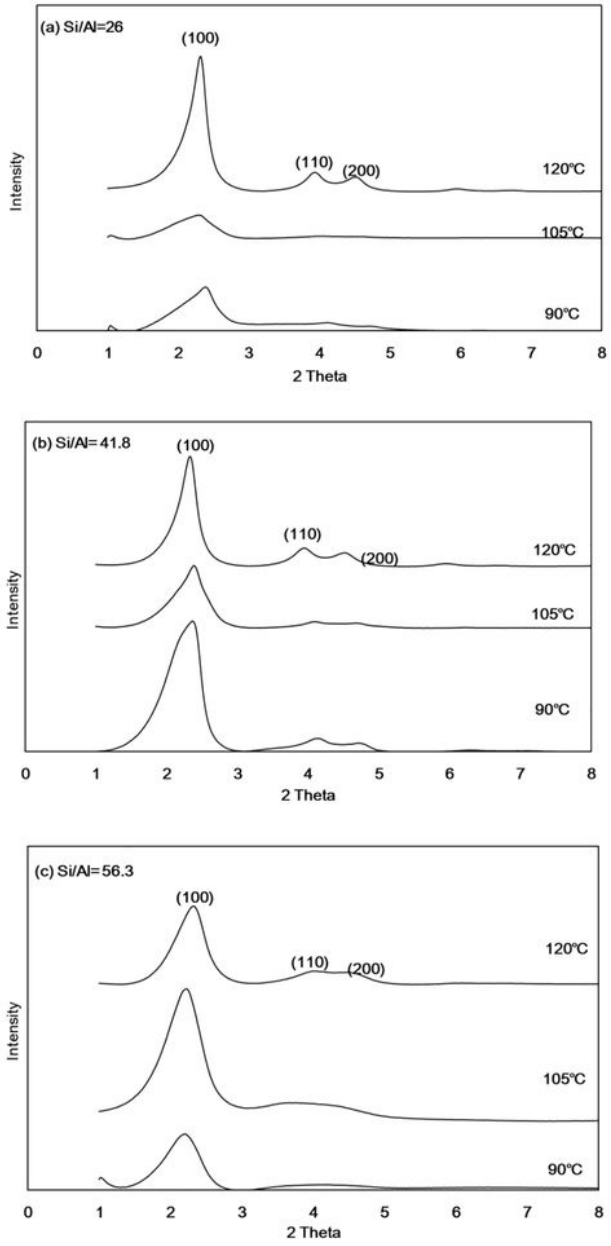

Figure 2

Crystal phase of synthesized Al-MHCM. (a) Si/Al= 26 (b) Si/Al= 41.8 (c) Si/Al= 56.3

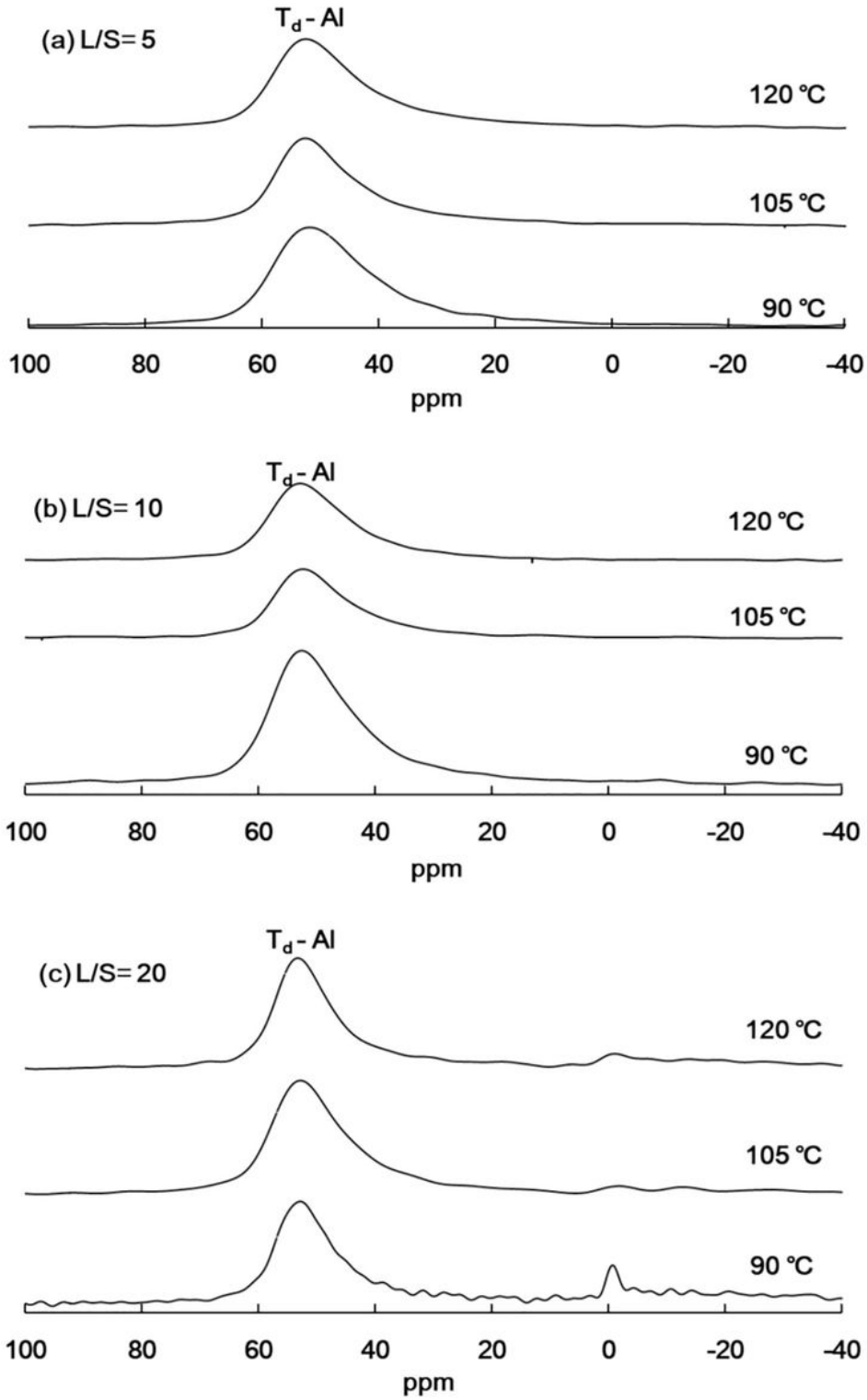

Figure 3

The 27Al NMR spectrum of the synthesized Al-MHCM. (a) Si/Al= 26；(b) Si/Al= 41.8；(c) Si/Al= 56.3

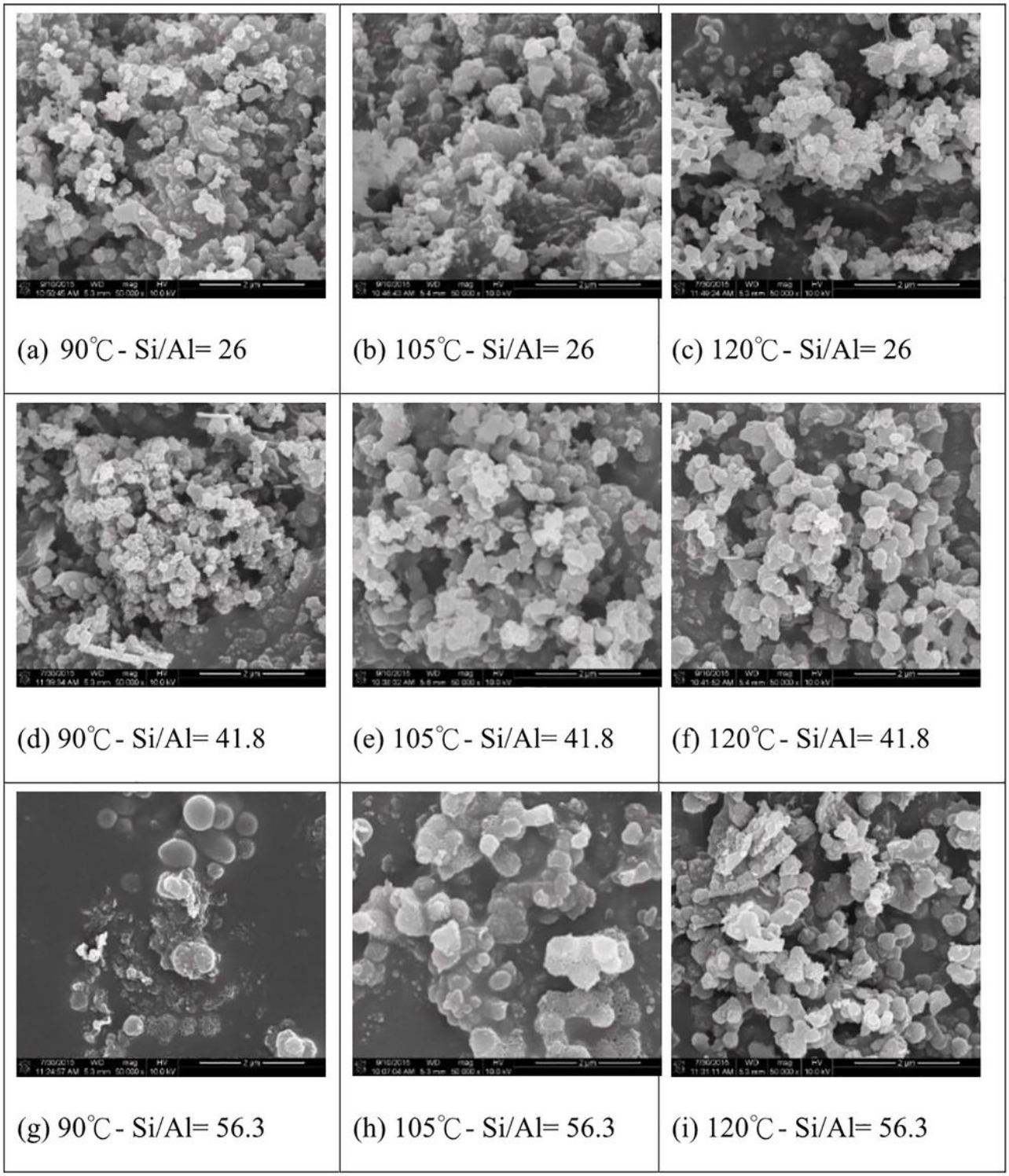

Figure 4

The SEM images of the synthesized Al-MHCM.

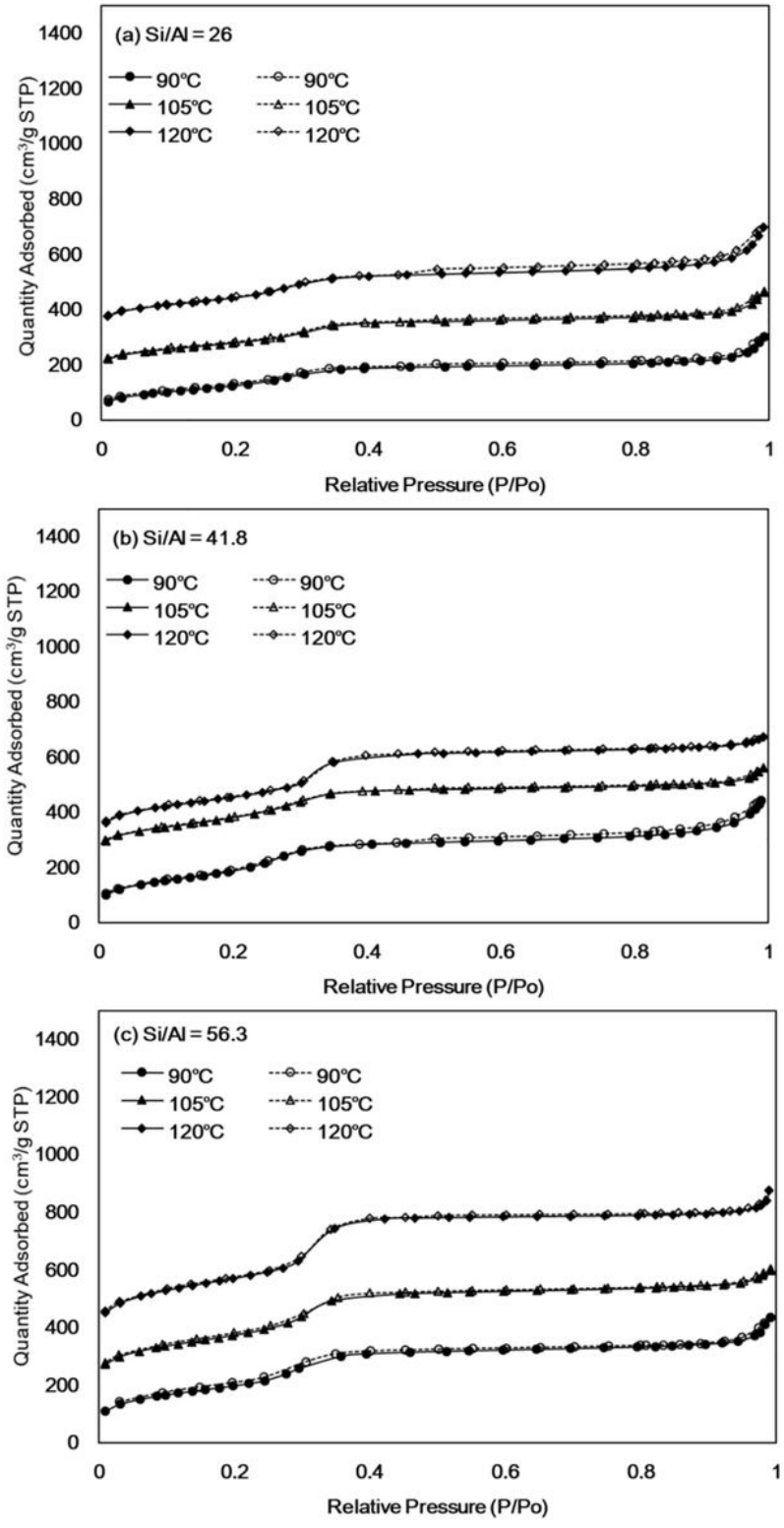

Figure 5

The N2 adsorption-desorption isotherm curves of the synthesized Al-MHCM. (a) Si/Al= 26 (b) Si/Al= 41.8 (c) Si/Al= 56.3

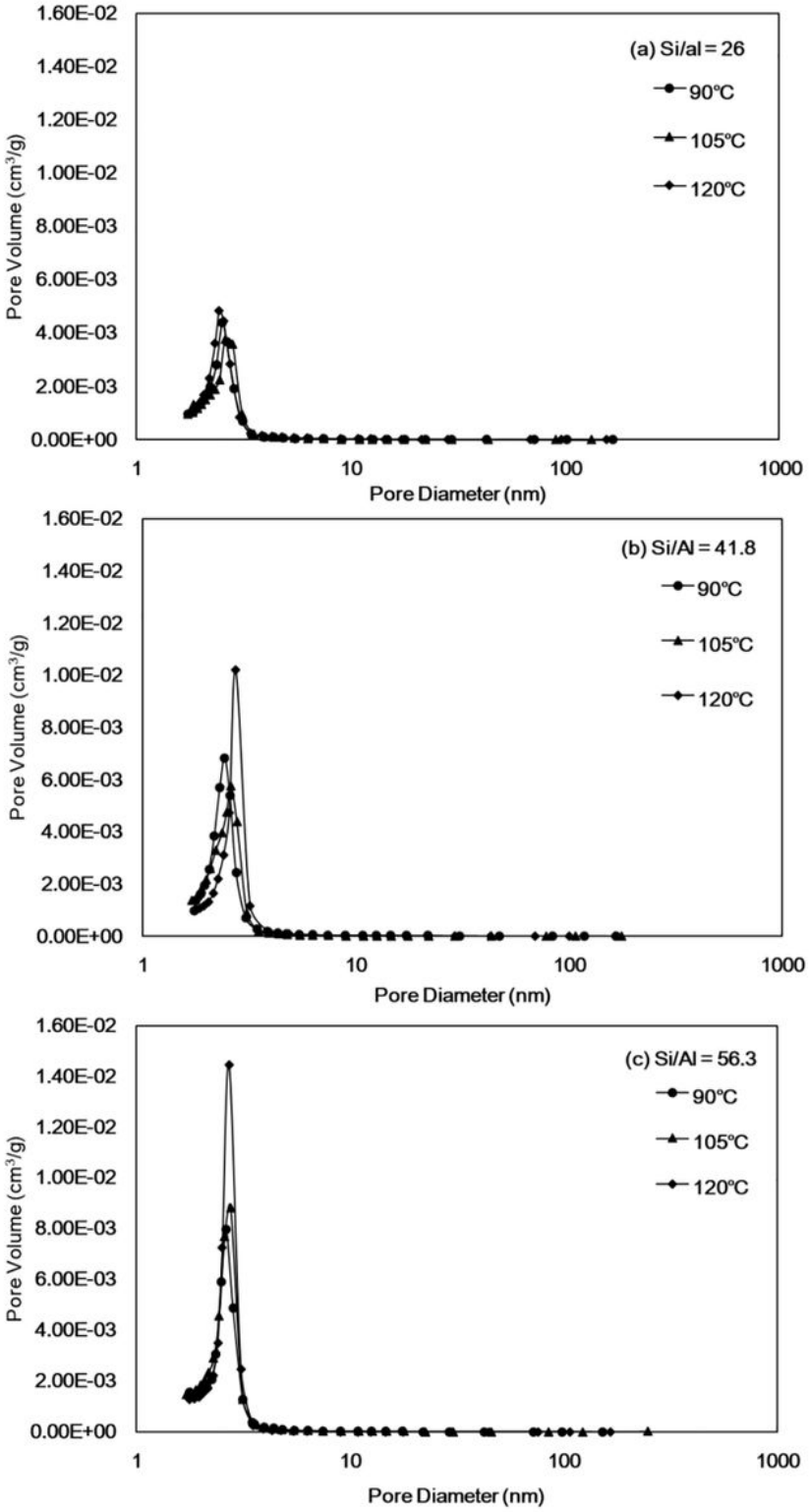

Figure 6

The total pore volume and pore diameter calculated of the synthesized Al-MHCM. (a) Si/Al= 26 (b) Si/Al= 41.8 (c) Si/Al= 56.

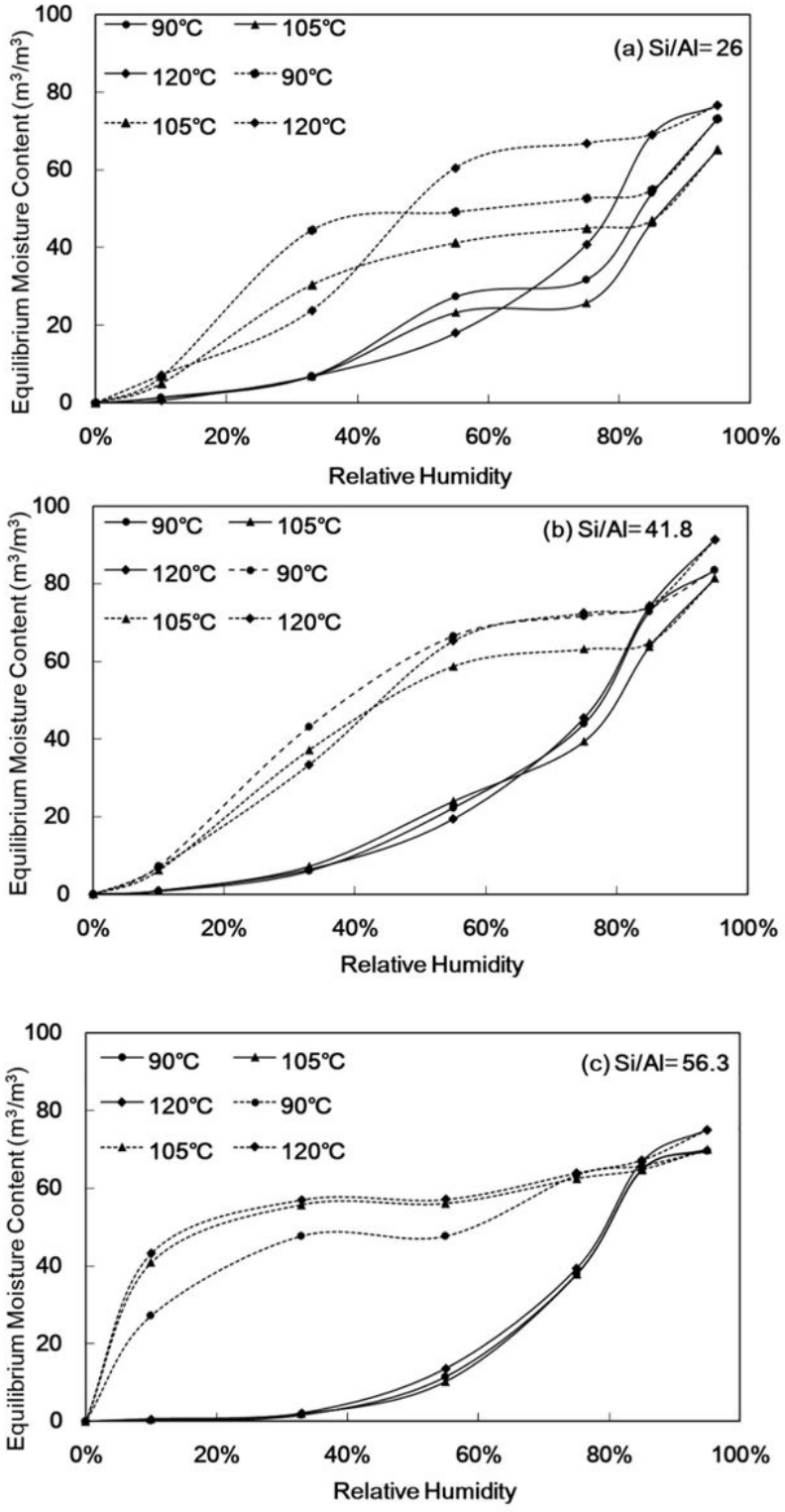

Figure 7

The 24-hour equilibrium moisture content curve of the synthesized Al-MHCM. (a) Si/Al= 26；(b) Si/Al= 41.8；(c) Si/Al= 56.3

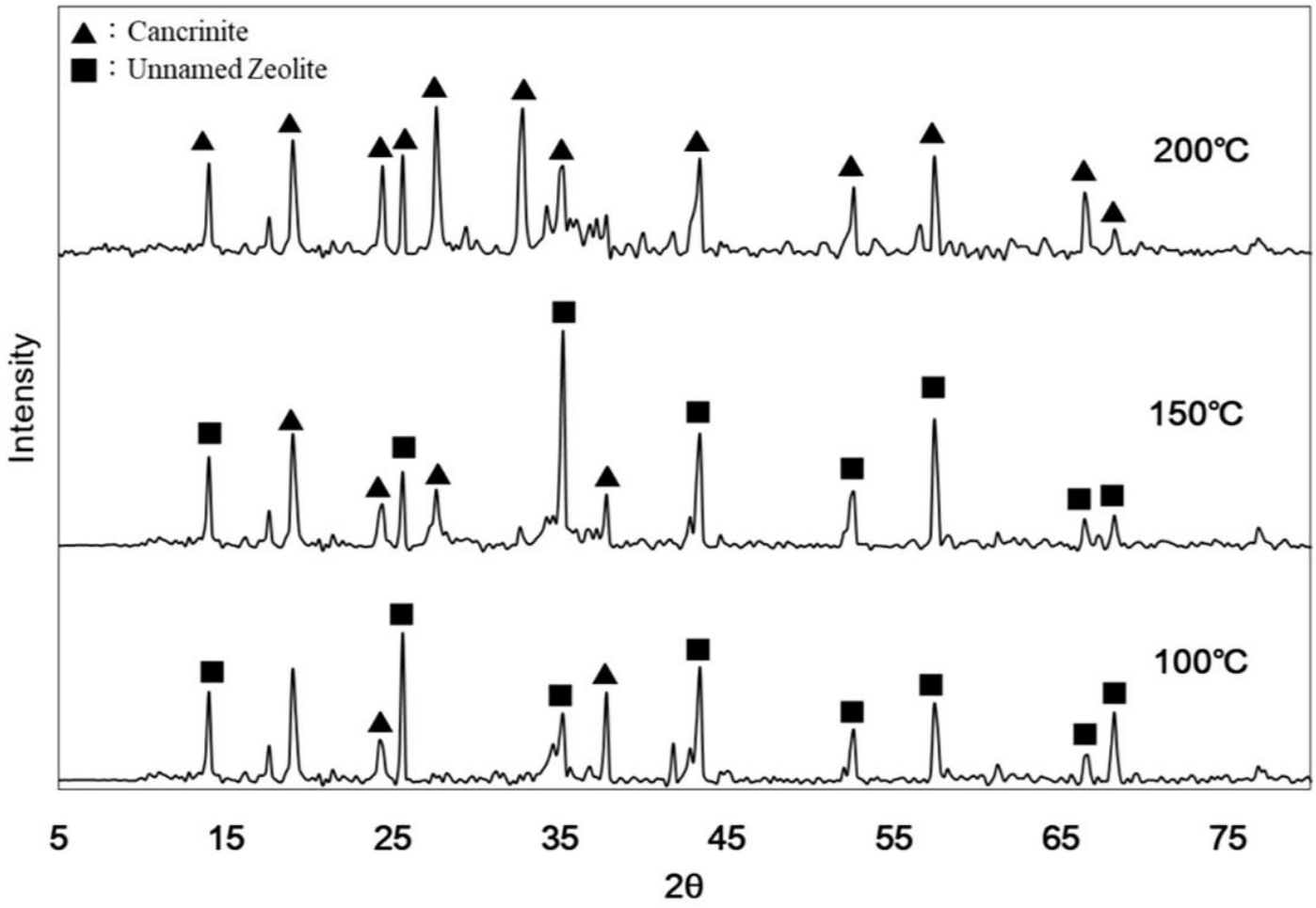

Figure 8

The XRD crystal phase of the synthesized microporous zeolite.